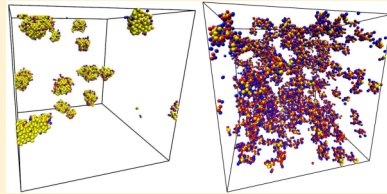


Lattice Model for Silica Polymerization: Monte Carlo Simulations of the Transition between Gel and Nanoparticle Phases

Mohammad Navaid Khan,[†] Scott M. Auerbach,^{*,‡} and Peter A. Monson^{*,†}

[†]Department of Chemical Engineering and [‡]Department of Chemistry, University of Massachusetts, Amherst 01003, United States

ABSTRACT: We present Monte Carlo simulations of a lattice model describing silica polymerization with an emphasis on the transition between gel states and nanoparticle states as the pH and silica concentration are varied. The pH in the system is controlled by the addition of a structure-directing agent (SDA) of the type $\text{SDA}^+(\text{OH}^-)$. The silica units are represented by corner-sharing tetrahedra on a body-centered cubic lattice and the SDA^+ species by single sites with near-neighbor repulsions. We focus on two systems: one with a low silica concentration with composition comparable to that of the clear solution silicalite-1 zeolite synthesis and a high silica concentration system that leads to gel states. In the dilute system, clusters have a core–shell structure, with the core predominantly comprised of silica with some SDA^+ cations, surrounded by a shell of only SDA^+ cations. Moreover, the average cluster size gradually decreases from 2 to 1.6 nm with increasing pH. The concentrated system forms a gel that remains stable to increasing pH up to about 9.2. At pH values in the range of 9.2–10, the gel transforms to nanoparticles of size around 1.0 nm, surprisingly smaller than those in the dilute system. We also study the evolution of the Q_n distribution (a measure of the silica network structure) for both systems and obtain good agreement with ^{29}Si NMR data available for the concentrated system.



1. INTRODUCTION

Sol–gel processing is an important technology used in the production of thin films, fibers, preforms, and nanoporous materials such as zeolites.^{1,2} Zeolites are crystalline aluminosilicates with extensive applications as adsorbents, catalysts, and ion exchangers.² All-silica zeolite frameworks such as silicalite-1 can be synthesized by sol–gel processing in aqueous media using a silica source and structure-directing agents (SDAs).³ A fundamental understanding of the synthesis process of such materials would enable the prediction of various properties such as pore size, framework type, and surface structure. A central component of zeolite synthesis is the polymerization of silica that produces both sols (nanoparticles) and gels (percolating networks). This paper is concerned with the modeling of silica polymerization under various conditions of pH and silica concentration to elucidate both kinds of structures that arise during sol–gel processing.

Our particular focus is on the formation of silicalite-1 because this represents a relatively well studied zeolite synthesis involving sols, i.e., suspended nanoparticles at short times that evolve with time and/or heat into zeolites.⁴ This pure silica form of the MFI zeolite framework contains parallel straight channels in one direction and zigzag channels perpendicular to the straight channels. It was first synthesized by Flanigen et al.³ by hydrothermal crystallization of a reactive form of silica in the presence of tetrapropylammonium cations as SDA at 100–200 °C and pH near 10. Eventually, the SDA cations occupy the channel intersections and are removed by calcination in the presence of air at 500–600 °C to yield microporous silicalite-1 crystals. Studies of the formation mechanism of silicalite-1 crystals^{4–13} have shown that the process involves an intermediate nanoparticle phase that is believed to play an important role in the nucleation process of these crystals.⁴

Scattering techniques, such as small-angle X-ray scattering (SAXS) and small-angle neutron scattering (SANS), suggest that these silica–SDA nanoparticles possess a core–shell-type structure.¹⁴ The core of the nanoparticles is hypothesized to be comprised primarily of silica, enveloped by a shell of cations. These particles, after being aged for a long period (~200 days), aggregate to give rise to a population of larger particles that contain the X-ray diffraction signature of silicalite-1 crystals.⁴ Yang et al.¹⁰ studied this system with the same components but at higher density and showed using SAXS that the nanoparticle size decreases with an increase in the concentration of SDA cations. However, the structure and morphology of these nanoparticles remain poorly known. Understanding the detailed structures of such nanoparticles would yield unprecedented insight into the early stages of zeolite formation.

In contrast to the high-pH behavior, at low pH near the isoelectric point of silica (pH ≈ 2–3¹⁵), an aqueous silica solution evolves into a disordered state of condensed silica networks. Carman¹⁶ proposed that the formation mechanism of such networks is a two-stage process. In the first, initially formed $\text{Si}(\text{OH})_4$ condenses to form colloidal particles. In dilute solution, particle aggregation may occur but does not lead to percolating networks, characteristic of gels. However, at a higher concentration of silica, these networks link into a continuous, relatively rigid material that ultimately percolates the system, leading to gelation. Devreux et al.¹⁷ studied the evolution of such aqueous silica networks using ^{29}Si NMR. They observed the evolution of the Q_n (the fraction of silicon atoms connected to n bridging oxygen atoms) distribution both

Received: May 20, 2014

Revised: July 8, 2014

Published: August 20, 2014

with time and with degree of condensation. Their results provide an excellent test for models of silica polymerization.^{18–20} Capturing the nature of the transition between nanoparticle and gel states of silica provides an important target for molecular modeling.

The polymerization of silica exhibits a complex interplay of several phenomena such as condensation/hydrolysis chemistry, acid–base equilibrium, metastability, and phase separation.^{21–23} Furthermore, SDA⁺ cations present in the system can influence the process via electrostatic interactions. Molecular modeling can potentially provide useful insights into the thermodynamic behavior of such systems, especially considering that silica networks often fall into the nanoscale blindspot between NMR (≤ 1 nm) and X-ray (≥ 50 nm). Researchers have employed simulation techniques such as molecular dynamics (MD) and Monte Carlo (MC) simulations to investigate the phenomena of silica polymerization under various conditions. Garofalini and co-workers^{24,25} studied the kinetics of silica polymerization using MD simulations and predicted that chains form at an early stage followed by ring formation. Rao et al.²⁶ performed large-scale MD simulations to find that the initial stages of polymerization are dominated by Ostwald ripening²² followed by cluster aggregation at longer times. The computational limitations of the models and MD, however, restricted such studies to relatively small system sizes, short times, and high temperatures to allow chemical bond breaking and re-forming.

To simulate silica polymerization under ambient conditions, Wu and Deem²⁷ used MC simulations to model silicate cluster formation. Using novel MC moves, they estimated the nucleation barrier for silica crystallization to be on the order of $10^2 k_B T$ and the critical nucleus size to be ~ 50 silicon atoms. Malani et al.^{18,19} developed a model of silica sampled with specialized MC simulations under ambient conditions at the isoelectric point, reproducing the measured Q_s evolution using specialized MC moves allowing oligomerization, ring formation, and cluster aggregation. Despite this progress, off-lattice simulations have yet to describe the crystallization of silica.

Recently we deployed lattice models to study silica polymerization at the isoelectric point ($\text{pH} \approx 2$),²⁰ and also spontaneous formation of nanoparticles at high pH ($\text{pH} \approx 10$) in clear solution synthesis of silicalite-1.²⁸ These models have also been applied to simulate the spontaneous formation of MCM-41 mesoporous silica materials²⁹ and the crystallization of microporous zeolite analogues.³⁰ Here, we extend these studies across the pH range and study the distinction between the nanoparticles formed at low and high silica concentrations. We have used an atomic representation of corner-sharing silica tetrahedra on a body-centered cubic (bcc) lattice.²⁸ The condensation reaction was modeled by simultaneous occupancy of hydroxyl groups from different tetrahedra on the same lattice site. Jin et al.²⁰ used this representation to predict network formation at the isoelectric point. Their results for the evolution of the Q_s distribution agree well with data from ^{29}Si NMR experiments.¹⁷ However, the phenomena of silica polymerization for various pH values and silica concentrations remain to be explored. In particular, it is unclear whether the gel transforms smoothly or abruptly to nanoparticles as the pH is increased and whether the nanoparticles are similar in size for systems with low and high silica concentrations. We address this issue by introducing a salt of type SDA^{+(OH⁻)} in our system to change the pH. The cation, SDA⁺, is represented as a single site on the lattice with near-neighbor repulsions accounting for its size. We impose an orientation-dependent

interaction of SDA⁺ with the anionic portion of Si(OH)₃O⁻ to mimic electrostatic charge balance. In this work we study low and high silica concentration systems and find the surprising result that the nanoparticles for the dilute silica system are larger than those in the concentrated system.

The outline of the paper is as follows. In section 2, we discuss the model. In section 3, we describe the simulation techniques used. In section 4, we present our results, first for a low silica concentration system and then for a high silica concentration system. In section 5, we compare our findings with those from experiments. Finally, in section 6, we present a summary of our results and conclusions.

2. MODEL

The objective of the present work is to study the process of silica polymerization over the pH spectrum. We aim to model this process using a simple model with enough detail to qualitatively reproduce and predict the experimental observations^{14,17,31} while at the same time not being overly complicated so as to restrict our study to smaller systems. To achieve this, we have developed an atomic lattice model to study the polymerization process. Such a model helps us to overcome the computational challenges involved in studying silica polymerization.³²

We follow closely the earlier work of Jin et al.²⁰ The silica source is chosen to be tetraethyl orthosilicate [Si(OC₂H₅)₄ or TEOS], and we assume that it hydrolyzes completely into a molecule of silicic acid and four molecules of ethanol. For simplicity, we do not distinguish between water and ethanol molecules, but rather we treat them as “solvent”. The pH of the system is controlled by adding a structure-directing agent of type SDA^{+(OH⁻)}. We assume complete dissociation of SDA^{+(OH⁻)} into SDA⁺ and OH⁻. Under such conditions, OH⁻ deprotonates the neutral silica monomer [Si(OH)₄] to produce an ionic silicate monomer [Si(OH)₃O⁻]. We assume that any remaining OH⁻ in the system goes to determine the pH. The cationic species (SDA⁺) can vary from a sodium cation (Na⁺)²¹ to a tetrapropylammonium cation [N(C₃H₇)₄⁺ or TPA⁺], which is used in the synthesis of silicalite-1.³³

We chose the bcc lattice, which can be viewed as two interpenetrating diamond sublattices, as a model for silica. We adopt an atomic representation of silica on a bcc unit cell.²⁰ The silicon atom, treated as a single site, is located at the center of the unit cell, whereas the hydroxyl groups, also treated as single sites, occupy either of the diamond sublattices. The neutral silica monomers ($\equiv\text{SiOH}$, also denoted as “SN”) and the ionic silica monomers ($\equiv\text{SiO}^-$, denoted as “SI”) are both represented by the bcc unit cell, as shown in Figure 1a,b.

To keep the model as simple as possible, we adopt a coarse-grained picture of the cation by representing it as a single site

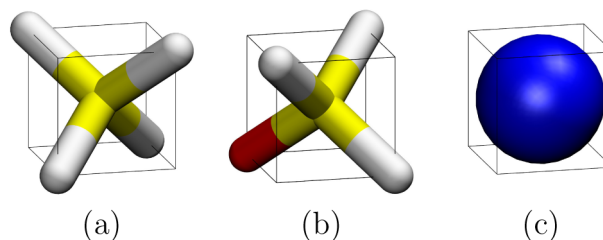
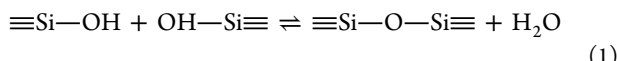


Figure 1. Representation of various species on the lattice: (a) neutral silica ($\equiv\text{SiOH}$); (b) ionic silica ($\equiv\text{SiO}^-$); (c) cation (SDA⁺).

with near-neighbor repulsions accounting for its size as shown in Figure 1c. In future work we will investigate more complex models of the SDA^+ cation. We represent water and ethanol molecules as vacant sites on the lattice.

2.1. Neutral Polymerization. The isoelectric point for silica, i.e., the pH at which the charge on silica vanishes, has been observed to be in the range of 2–3.¹⁵ Under such conditions and at room temperature, the kinetics of condensation are slow and changes in the silica network structure of the system can be observed spectroscopically (e.g., with ^{29}Si NMR).¹⁷

We adopt a simplified view of the reactions occurring in such a system; we define the neutral polymerization reaction as



Here a silica cluster ($\equiv\text{SiOH}$) reacts with another silica cluster, resulting in the formation of a bridging oxygen and liberation of a water molecule, treated as a lattice vacancy. We model this reaction in our system allowing two tetrahedral vertices to share the same site with an accompanying lowering of the energy. This energy lowering represents the exothermicity of the condensation reaction and has been calculated using density functional theory coupled with the continuous dielectric model.³³ The resulting configuration is shown in Figure 2.

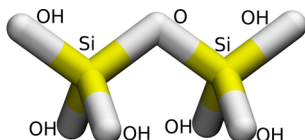
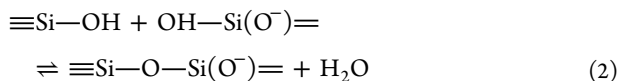


Figure 2. Result of neutral polymerization producing a bridging oxygen between two SN molecules.

2.2. Alkaline Polymerization. As mentioned earlier, the pH of the system can be controlled by introducing a base of the type $\text{SDA}^+(\text{OH}^-)$. In the presence of $\text{SDA}^+(\text{OH}^-)$, the hydroxide ion (OH^-) can deprotonate an SN, resulting in a singly deprotonated silicate species $[\text{Si}(\text{OH})_3\text{O}^-]$ or SI. To further simplify our model, we consider only singly ionized monomers. Although doubly ionized silica $[\equiv\text{Si}(\text{O}^-)_2]$ has been shown to exist at sufficiently high pH,^{21,22,34} it has been hypothesized to remain inert in the polymerization process.³⁵



Therefore, in the presence of $\text{SDA}^+(\text{OH}^-)$, we need to consider two additional types of polymerization reactions: (i) SN reacting with SI to form a bridging oxygen as illustrated in Figure 3 and (ii) condensation between two SI molecules to yield $\equiv\text{Si}(\text{O}^-)\text{OSi}(\text{O}^-)\equiv$. We assume that the electrostatic

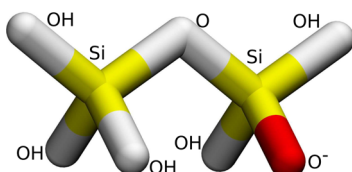


Figure 3. Alkaline polymerization forming a bridging oxygen between SN and SI molecules.

repulsion between two SI molecules is strong enough to prohibit their condensation from taking place.

Moreover, O^- is prohibited from forming a bridge with a hydroxyl group of another silica species. Such a reaction would result in the liberation of a hydroxide ion (OH^-) instead of a water molecule, which is thermodynamically unfavorable.

2.3. Interaction of Cations. As a base case model, the cation (SDA^+) in our model is treated as a single site with excluded volume. We will consider more complex SDA^+ models in a forthcoming paper. The excluded volume is accounted for by imposing near-neighbor repulsions (between the cation site and its first nearest neighbors). Such a model may mimic a sodium cation or a tetralkylammonium cation depending upon the range of repulsions.

2.4. Parameters. With four distinct species in our system, SN, SI, SDA^+ , and H_2O , there would be ten interaction energies, SI—SN , SI—SI , SN—SN , SI—SDA^+ , SN—SDA^+ , $\text{SN—H}_2\text{O}$, $\text{SI—H}_2\text{O}$, $\text{SDA}^+—\text{H}_2\text{O}$, $\text{SDA}^+—\text{SDA}^+$, and $\text{H}_2\text{O—H}_2\text{O}$. The Hamiltonian of the system is given by

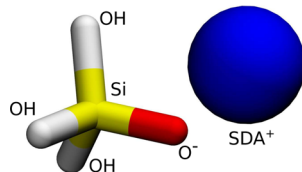
$$H = \sum_{i=1}^m \sum_{j \geq i}^m C_{i,j} \varepsilon_{i,j} \quad (3)$$

where m is the number of components in the system, $C_{i,j}$ is the total number of interaction contacts between components i and j , and $\varepsilon_{i,j}$ is the corresponding interaction energy. Jorge et al.²⁸ defined the reduced temperature of such a system as $T^* = k_{\text{B}}T / |\varepsilon_{\text{SN,SN}}|$. Jin²⁰ studied the change in solubility of an all-silica system with temperature and obtained $\varepsilon_{\text{SN,SN}} = -3.4$ kcal/mol, which gives the value of room temperature as $T^* = 0.15$. We use this value of T^* in the present work.

We now focus on specifying the remaining interaction energies in the system. The nature of the SI—SN interaction should be attractive, as exothermic condensation takes place between SN and SI. Consistent with our previous work,²⁸ we have assigned $\varepsilon_{\text{SI,SN}} = 0.8\varepsilon_{\text{SN,SN}}$. As stated above, we assume that the SI—SI condensation reaction does not contribute significantly to the polymerization process; hence, we assign $\varepsilon_{\text{SI,SI}} = 0$, which neither precludes nor favors this process.

In the present work, the SDA^+ cation occupies a single site and has first-neighbor repulsion with every species. This makes the size of the cation comparable to the size of the silica monomer, i.e., approximately 3.2 Å in diameter, or that of a tetramethylammonium (TMA) cation.³⁶ The interaction between cations is dominated by electrostatic repulsion; thus, we assume an infinite repulsion between cations extending to the first neighboring sites. The cation–cation repulsion is assumed to be short ranged in our model because of Debye–Hückel screening.²¹ The interactions between SI and SDA^+ are attractive because of electrostatic attraction. The interaction depends upon the orientation of SI and was calculated to be higher than the condensation energy of silica.³⁷ Therefore, consistent with our previous work, we have assigned $\varepsilon_{\text{SI,SDA}^+} = 2.0\varepsilon_{\text{SN,SN}}$. To maintain local charge balance, we impose the condition that a molecule of SI interacts with only one molecule of SDA^+ and vice versa, as shown in Figure 4. The interactions between SDA^+ and SN are set to zero for simplicity. Moreover, we assume for simplicity that the interaction of water (i.e., vacancies) with all the species is zero.

Using all the above simplifications, the Hamiltonian now takes the form

Figure 4. Interaction of SDA^+ with O^- of an SI monomer.

$$H = \sum_{i=1}^3 \sum_{j \geq i}^3 C_{i,j} \epsilon_{i,j}$$

where the indices corresponding to 1, 2, and 3 represent SI, SN, and SDA, respectively. The interaction strengths are given in Tables 1 and 2.

Table 1. Interaction Energies for First Neighbors

	SI	SN	SDA^+
SI	0.0	-0.8	∞
SN	-0.8	-1.0	∞
SDA^+	∞	∞	∞

Table 2. Interaction Energies for Second Neighbors

	SI	SN	SDA^+
SI	0.0	0.0	-2.0
SN	0.0	0.0	0.0
SDA^+	-2.0	0.0	0.0

3. SIMULATION TECHNIQUE

We use canonical ensemble Monte Carlo simulations to study the behavior of the system. We implement periodic boundary conditions on the boundaries of the lattice and start the simulation by placing molecules at random locations on the lattice. Next we attempt three kinds of moves to efficiently sample the different states of the system. The first move is translation, where we select a molecule at random and another site at random on the lattice. If the selected site is vacant, we attempt to move the molecule to the new site. The second move is a swap between two molecules, where we attempt to exchange two molecules selected randomly. The third kind of move is the rotation of a silica tetrahedron. In the case of SN we attempt to rotate the tetrahedron by randomly assigning it to the other diamond sublattice of the unit cell, whereas for SI we move O^- randomly on one of the eight first nearest neighbors and the hydroxyl groups accordingly. All moves are accepted or rejected on the basis of the Metropolis condition.³⁸ An MC step consists of N trial moves, where N is the number of molecules in the system. A trial move is comprised of an attempted translation, an attempted swap, and an attempted rotation. We study cluster size statistics using the Hoshen–Kopelman algorithm,³⁹ where we consider two silica monomers to be part of the same cluster if they are connected by a bridging oxygen atom. In determining cluster statistics, we (somewhat arbitrarily) define aggregates that have greater than 15 silica units as a cluster.

We have studied both dilute and concentrated systems with respect to silica concentration. The dilute system has the composition 40TEOS: $x\text{SDA(OH)}$:9500 H_2O , whereas the concentrated system has the composition 25TEOS: $x\text{SDA(OH)}$:400 H_2O . Here, x is the mole proportion of

$\text{SDA}^+(\text{OH}^-)$. The lattice size in both the systems is $100 \times 100 \times 100$, which has been found sufficient in previous work.^{20,28} Length scales in the system are controlled by the Si–O bond length, which is approximately 1.6 Å. This makes the lattice dimension 18.5 nm in all the directions. Both the systems were studied for 10×10^6 MC steps, with equilibrium found to be attained after 5×10^6 MC steps for the low silica concentration system and 7×10^6 MC steps for the high silica concentration system.

The topology of silica networks changes significantly with pH. We study these changes by computing the variation in average cluster size with a change in the cation content. The diameter of a cluster can be calculated using the diameter of gyration:

$$D = 2 \sqrt{\frac{1}{2N^2} \sum_{j=1}^N \sum_{i=1}^N |\mathbf{r}_i - \mathbf{r}_j|^2}$$

where N is the number of silica units in the cluster and $|\mathbf{r}_i - \mathbf{r}_j|$ is the distance between the i th and j th silicon atoms belonging to the same overall cluster. We implement the minimum image convention to calculate distances between the silicon atoms. Next we calculate the mass average and mole average size for every cluster in the system according to

$$\langle \text{cluster size} \rangle^{\text{mole average}} = \frac{\sum_{k=1}^M D_k}{M}$$

$$\langle \text{cluster size} \rangle^{\text{mass average}} = \frac{\sum_{k=1}^M D_k N_k}{\sum_{l=1}^M N_l}$$

where M is the total number of clusters, N_l is the total number of silica units in cluster l , and D_k is the diameter of the k th cluster. It should be noted that we only consider silica molecules, and not SDA^+ species, while calculating the average cluster size. The ratio of the mass to mole average cluster size gives the polydispersity ratio,⁴⁰ which is a measure of the heterogeneity in the cluster size distribution, with monodisperse distributions showing a polydispersity ratio of unity and polydisperse systems showing a polydispersity ratio exceeding unity.

We also compute the pair distance distribution function (PDDF) by plotting a histogram of distances between silicon atoms in a cluster for comparison with distributions extracted from small-angle X-ray scattering and small-angle neutron scattering data. The structural properties of networks can be obtained by computing the Q_n distribution, which gives the fraction of Si atoms bonded to n bridging oxygens. Harris and co-workers^{41,42} measured ^{29}Si NMR chemical shifts in aqueous silicate solutions. Their findings indicate that ^{29}Si chemical shifts are very different for neutral and anionic silica species,²² suggesting that the chemical shifts that determine the Q_n distributions for our system are dominated by connectivities around SN. Therefore, while calculating Q_n distributions, we only consider connectivities of silicon atoms around SN species in our simulations and ignore connectivities of silicon atoms around SI in our simulations. The normalization of the Q_n distribution is computed on the basis of the total SN present in the system. We also calculate the pH of the system, as detailed in the Appendix.

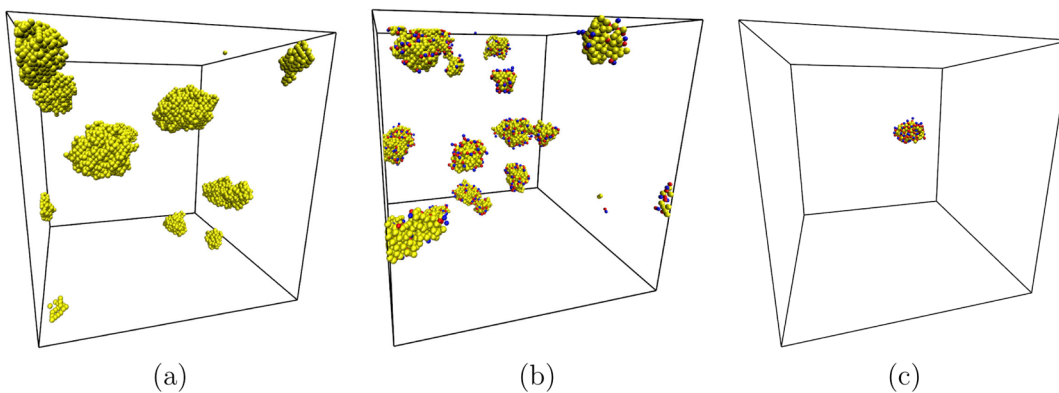


Figure 5. Snapshots of the system after 10×10^6 Monte Carlo steps with composition 40TEOS: x SDA(OH):9500H₂O: (a) $x = 0.0$; (b) $x = 9.0$; (c) $x = 38.0$. Key: yellow spheres, SN; red spheres, SI; blue spheres, SDA. Note that the snapshots show only clusters having 15 or more SN and SI tetrahedra.

4. RESULTS AND DISCUSSION

4.1. Dilute System. Fedeyko et al.¹⁴ characterized the intermediate nanoparticle phase observed during the synthesis of silicalite-1 using SAXS and SANS on a system dilute with respect to silica with the following composition: 40TEOS: x SDA(OH):9500H₂O. They hypothesized that the difference between the pair distance distribution functions obtained by SAXS and SANS may be evidence of the existence of a diffuse double layer around the silica clusters including SDA⁺ cations and compensating anions. They also proposed that the nanoparticles have a core–shell structure with silica in the core and SDA⁺ cations in the shell. We have modeled this composition to investigate whether a core–shell structure emerges in our simulations.

4.1.1. Snapshots. A series of system snapshots at various SDA⁺ mole fractions is shown in Figure 5, generated using the Visual Molecular Dynamics package.⁴³ The qualitative behavior of the simulations is similar to that in our earlier work on silica polymerization.²⁰ In each case, starting from a random initial configuration, the clusters grow with the phenomenon of Ostwald ripening,²² involving smaller clusters dissolving rapidly, adding their silica tetrahedra to larger clusters. In the absence of SDA⁺ cations, a nanoparticle phase is observed containing clusters of silica as seen in Figure 5a. As the SDA⁺(OH⁻) concentration is increased, more neutral silica molecules are deprotonated to ionic silica by the reaction mentioned in the Appendix. There exists a competition between the electrostatic attraction of SI–SDA⁺ and the condensation energy between silica molecules that leads to the formation of nanoparticles possessing core–shell structures. The cores of these nanoparticles have silica surrounded by a shell of cations as shown in Figure 5b. When the mole proportion of SDA⁺(OH⁻) reaches a value close to that of TEOS, virtually all silica is in the form of SI, and hence, no clusters are observed in the system.

We find under these dilute conditions that the concentration of silica is not high enough to produce percolating networks in our simulations. This suggests that we need to consider higher silica concentrations to observe the transition from nanoparticles to gels.

4.1.2. Cluster Statistics. Figure 6 shows the effect of the SDA⁺(OH⁻) mole fraction on the mass and mole average cluster sizes and also on the total number of clusters. Greater weights are assigned to larger clusters in the mass average cluster size calculation, making it greater than the mole average cluster size for which equal weights are assigned to each cluster.

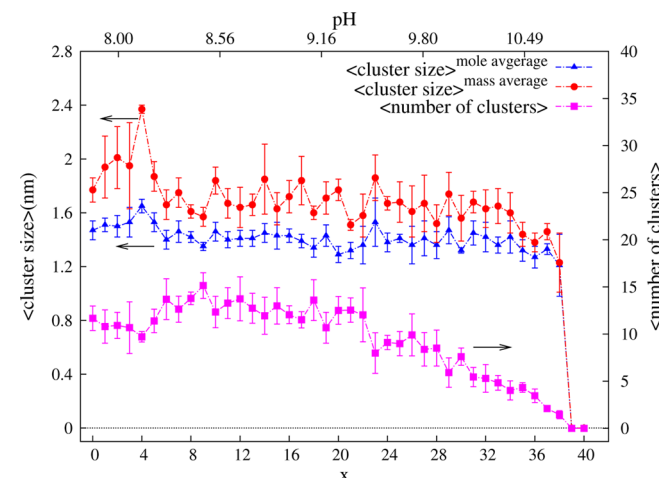


Figure 6. Effect of the SDA mole fraction on the cluster sizes and number of clusters in the system, giving a relatively monodisperse cluster size distribution with a polydispersity of 1.1–1.2.

We observe that both the average cluster sizes gradually decrease with an increase in the SDA⁺(OH⁻) mole fraction. As the amount of SDA⁺ increases, the amount of SI also increases because SDA⁺ carries the strong base which deprotonates SN to yield SI. The mass average cluster size obtained in our simulations (1.6–2.0 nm) is comparable to results from experiments performed at the composition 40TEOS:9SDA(OH):9500H₂O.¹⁴

Size distributions may be further understood by analyzing PDDFs shown in Figure 7, which reveals that as the mole fraction of SDA⁺(OH⁻) increases, the PDDF peak shifts to the left, indicating a gentle trend toward smaller clusters. Increasing the concentration of SI yields smaller clusters for two reasons: in contrast with SN, which is a tetravalent network-forming species, SI is only a trivalent network former, and SI–SI condensation is not driven by a favorable interaction because of electrostatic repulsion. The polydispersity, given by the ratio of the mass to mole average cluster sizes, falls in the range of 1.1–1.2 from these simulations, indicating reasonably monodisperse cluster size distributions. The tails of the PDDF curves are associated with the maximum cluster size in the simulations. The total number of clusters present in the system first increases weakly and then systematically decreases with x . However, the decrease after $x \approx 26$ is due to our definition of a

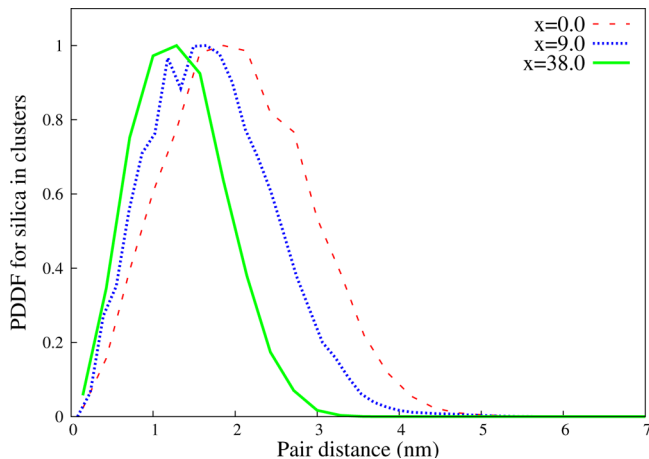


Figure 7. Pair distance distribution function at various SDA^+ concentrations for the dilute silica case, corresponding to the snapshots in Figure 5.

cluster as an aggregate with greater than 15 silica units. We note that the case of $x = 0$ ($\text{pH} \approx 2\text{--}3$) is treated separately when it comes to the pH calculation, as mentioned in the Appendix.

Fedeyko et al.¹⁴ measured the PDDF using SAXS and SANS scattering experiments. Because X-rays are scattered mostly by silica (higher electron density) whereas neutrons are scattered by both silica and SDA^+ species, we model the SAXS data by computing the PDDF including only silica and the SANS data by computing the PDDF including both silica and associated SDA^+ cations within each cluster. To compare our findings with these scattering experiment results, we have calculated the PDDF for silica, SDA^+ , and silica + SDA^+ as shown in Figure 8.

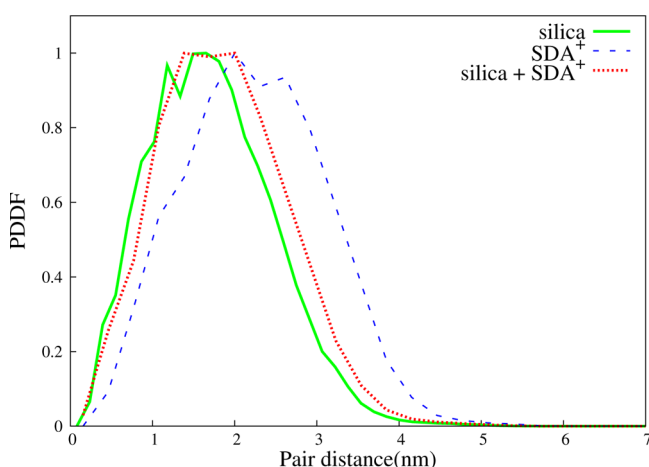


Figure 8. Pair distance distribution functions for silica, SDA^+ , and silica + SDA^+ at 40TEOS:9SDA(OH):9500H₂O.

The PDDF curves for silica and SDA^+ indicate a core of silica surrounded by a shell of SDA^+ cations. However, the PDDF for SDA^+ species also contains smaller pair distances than the average cluster size, suggesting that the SDA^+ cations are present inside the clusters as well. The difference between the PDDF of silica and the PDDF of silica + SDA^+ at higher pair distances is indicative of the presence of SDA^+ surrounding the cluster as predicted by Fedeyko et al.¹⁴ Overall, Figure 8 shows that SDA^+ species in our model are in both the core and shell of these core–shell nanoparticles.

4.1.3. Q_n Distribution. The Q_n distribution provides another structural descriptor of the connectivity around silicon atoms and is measured by ²⁹Si NMR.²¹ Figure 9 shows the evolution

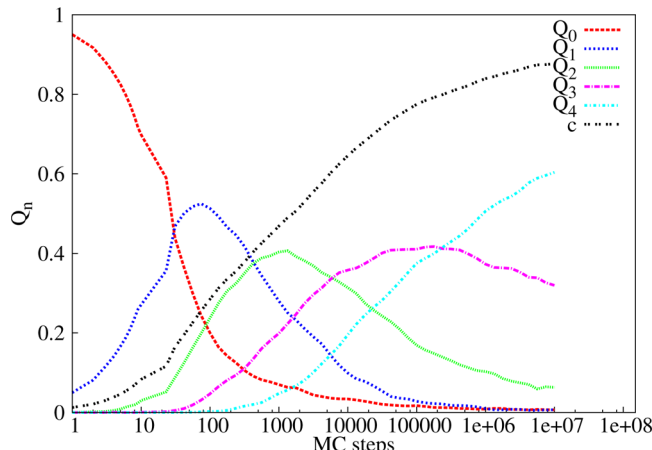


Figure 9. Evolution of the Q_n distribution with MC steps at 40TEOS:9SDA(OH):9500H₂O.

of the Q_n distribution with MC steps. We observe that Q_0 , the fraction of monomers in the system, monotonically decays as monomers combine to form higher order polymerized units. Q_1 , which is indicative of oligomers, peaks at approximately 100 steps. Q_2 , which accounts for rings and chains, peaks at 1000 steps. Q_3 is representative of silica units in small clusters and peaks around 100 000 steps. Q_4 , which accounts for condensed clusters, monotonically increases. The degree of condensation, defined as $c = 1/4 \sum_{n=0}^4 n Q_n$, is a monotonically increasing function of MC steps. The qualitative behavior of the curves in Figure 9 is similar to that observed in our previous work.²⁰

4.2. Concentrated System. Having established the existence of nanoparticles in the low silica concentration system, we now focus our attention on the high silica concentration system with the composition 25TEOS: $x\text{SDA(OH)}$:400H₂O, which has been used in previous experimental studies.³¹

4.2.1. Snapshots. A series of snapshots of the higher silica concentration system at various mole proportions of the cation is shown in Figure 10. At such a high silica concentration, the system would have a large number of molecules, which would be a hindrance in viewing the networks. To overcome this difficulty, we omit aggregates of 15 tetrahedra or smaller in Figure 10.

In the absence of cations ($x = 0$), we observe a large network that percolates the simulation cell as shown in Figure 10a. The spatial extent of this network is limited by the size of the system we study. The existence of such a network has been associated with gelation.²² As the cation content is increased, more SN is converted to SI according to the deprotonation reaction detailed in the Appendix. Moreover, since there is no attraction present between SI molecules, the amount of silicate anions present in the solution increases. This behavior is similar to that of the low silica concentration system we studied. The presence of the percolating network persists to high values of x ($x = 16.0$) as shown in Figure 10b. At even higher values of x ($x = 22.0$), we observe the nanoparticle regime. These nanoparticles are different from our predictions in the low silica concentration system: they are more numerous but smaller in size than those obtained at low silica concentrations. This is

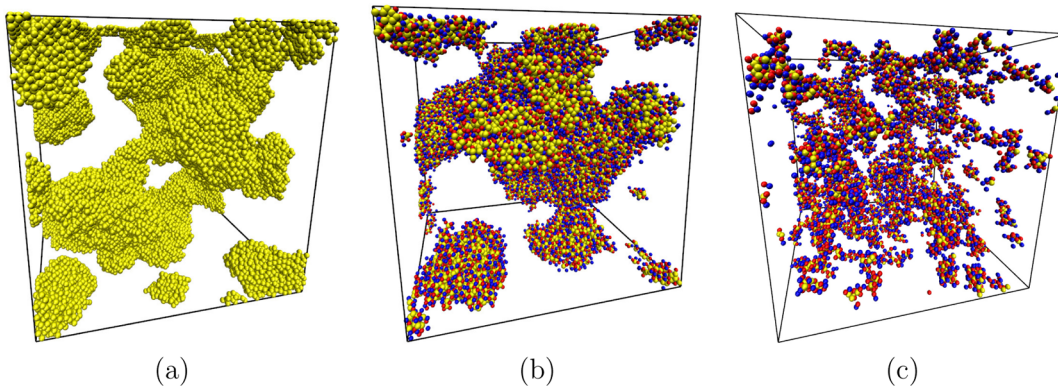


Figure 10. Snapshots after 10×10^6 MC steps with the composition 2STEOS: x SDA(OH):400H₂O: (a) $x = 0.0$; (b) $x = 16.0$; (c) $x = 22.0$. Only clusters of size 15 or bigger are shown here.

surprising as we may expect the nanoparticle size at higher silica concentration to exceed that at lower silica concentration.

4.2.2. Cluster Statistics. We now study cluster statistics as a function of the SDA⁺ mole fraction. Similar to Figure 6, we have computed the mass and mole average cluster sizes, shown in Figure 11. In contrast to Figure 6, we see in Figure 11 that

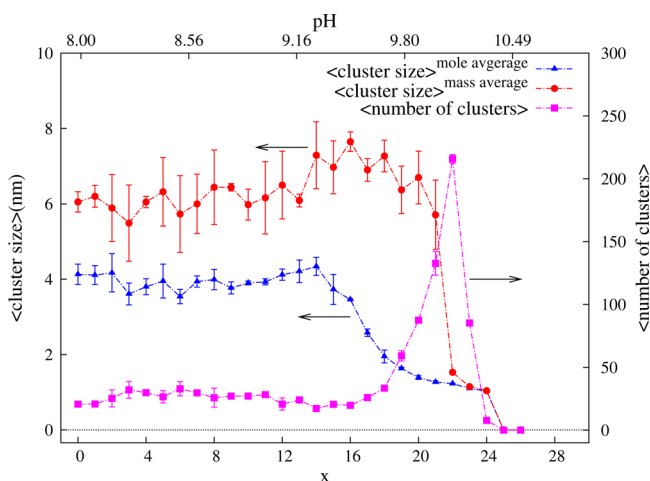


Figure 11. Average cluster size and number of clusters as a function of the SDA⁺ mole fraction at 2STEOS: x SDA(OH):400H₂O.

the mass average cluster sizes are significantly greater than the mole average values. This indicates high polydispersity of the clusters in this system. We observe two plateaus in the mole average cluster size with an increase in x . These plateaus may be misinterpreted as a gel regime for $0 \leq x \leq 15$ and a nanoparticle regime for $16 \leq x \leq 24$; however, the mass average cluster size suggests a different picture. It predicts a percolating network for compositions in the range of $0 \leq x \leq 21$, where the average cluster size is close to half the simulation cell size (~ 9.25 nm). Due to the high silica concentration, we do not observe independent clusters as in Figure 5, but rather we see clusters that are connected to each other by links of condensed silica. For $x \geq 22$, the mass average cluster size drops precipitously to a low value, suggesting the transition to the nanoparticle regime, where the size of the nanoparticles is ~ 1.0 nm. No clusters are observed for SDA⁺(OH⁻)/TEOS ≥ 1 ($x \approx 25$). The polydispersity drops to nearly unity for $22 < x < 25$, indicating a rather monodisperse collection of relatively small silica nanoparticles.

Similar conclusions can be derived from Figure 12, which shows the pair distance distribution function. At $x = 0.0$ and $x =$

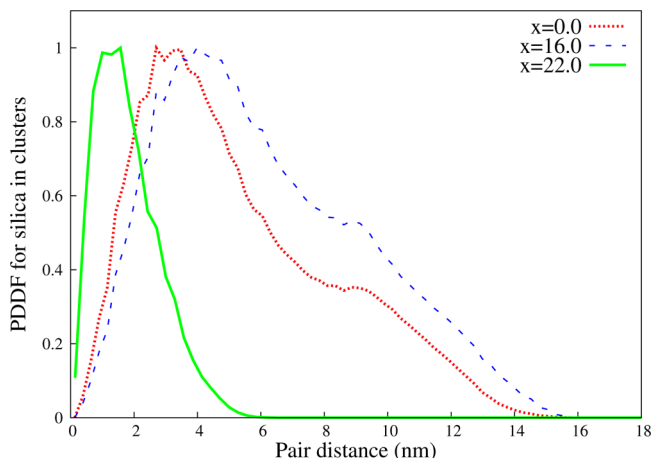


Figure 12. Pair distance distribution function for the gel ($x = 0$), transition ($x = 16.0$), and nanoparticle ($x = 22.0$) states.

16.0, the tails of the distribution functions are greater than half the system dimension, indicative of percolation. At $x = 22.0$, the function resembles that of Figure 7, with the peak at a lower distance suggesting that the cluster sizes are smaller than those of the low silica concentration system.

4.2.3. Q_n Distribution. The evolution of the Q_n distribution with MC steps for the concentrated system is shown in Figure 13. We observe that Q_0 monotonically decays as the monomers combine to form higher order polymerized units. Q_1 (oligomers) peaks at approximately 10 steps, Q_2 peaks after 100 steps, and Q_3 peaks around 7000 steps. These results are qualitatively similar to those described above for the low silica concentration system. This finding suggests that the Q_n distribution is relatively insensitive to differences in silica polymerization arising from different silica concentrations.

5. COMPARISON WITH EXPERIMENTS

We present a comparison of our calculated Q_n distributions with those from dilution studies (increase in the water content instead of decrease in the SDA⁺(OH⁻) mole fraction) by Follens et al.³¹ in Figure 14. They measured Q_1 , Q_2 , Q_3 , and Q_4 values using ²⁹Si NMR during the clear solution synthesis of silicalite-1 under various conditions. The vertical line represents the degree of condensation at which the Q_n measurements were

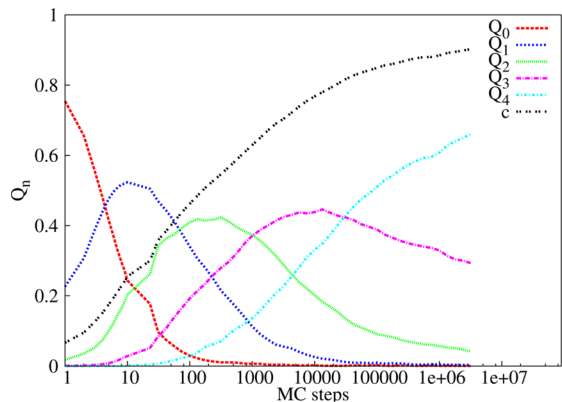


Figure 13. Evolution of the Q_n distribution with MC steps at 25TEOS:22SDA(OH):400H₂O.

made, and the colors of the points on the line correspond to the respective Q_n values. It should be noted that the experimental values of Q_2 and Q_3 are the same (~ 0.171) in Figure 14a. We observe that our simulations reproduce the Q_n values reasonably well, suggesting that our model captures aspects of the silica polymerization mechanism in the high water content systems (Figure 14b–d) to a good extent. However, in the low water content system (Figure 14a), the model gives only a qualitative agreement with the Q_n values. We believe this may

be due to the assumptions made about the various interactions with water being set to zero.

6. SUMMARY AND CONCLUSIONS

Building on previous work,²⁰ we have further developed and applied a lattice model for silica polymerization over a broad pH range and for different silica concentrations. We represent silica monomers as rigid tetrahedra on a unit cell of a bcc lattice, where a silicon atom occupies the body center of the unit cell and hydroxyl groups are at the vertices. The pH in the system is controlled by the amount of SDAs carrying a strong base in the form of $SDA^+(OH^-)$. The SDA cations, SDA^+ , are represented as single sites on the lattice with first-neighbor repulsions with every species. We have modeled the condensation reaction via double occupancy of hydroxyl groups at a single lattice site, hence representing corner-sharing tetrahedra. We also considered short-ranged attractions between O⁻ of SI and SDA⁺. As with our previous work with this model, we have imposed energy penalties on three- and four-membered rings and have prohibited the formation of two-membered rings. With appropriate interaction energies between components, this model has been found to elucidate the silica polymerization process over a broad pH range.

We have applied this model to two systems: systems with low and high silica concentrations.

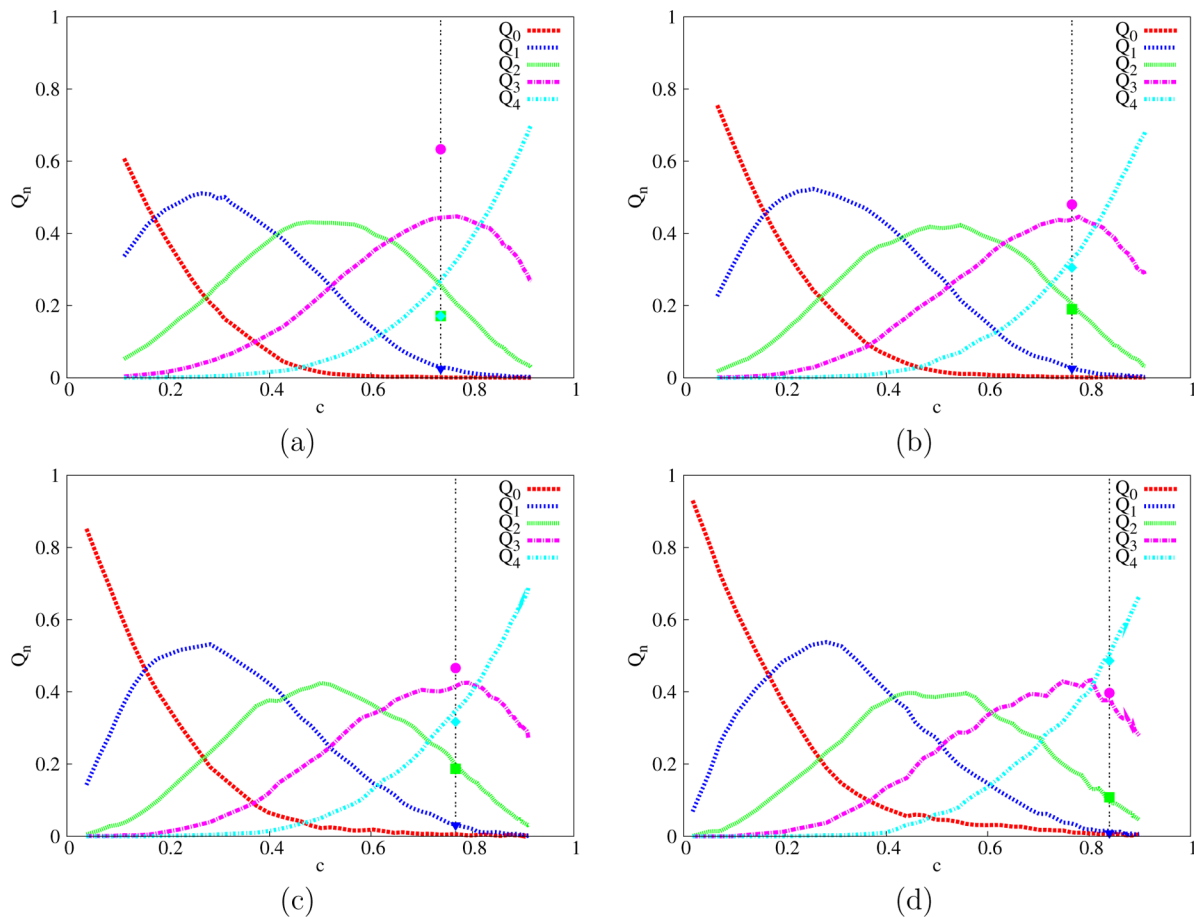


Figure 14. Q_n distribution compared with that from experiments:³¹ (a) 25TEOS:9SDA(OH):400H₂O; (b) 25TEOS:9SDA(OH):900H₂O (c) 25TEOS:9SDA(OH):1900H₂O; (d) 25TEOS:9SDA(OH):4000H₂O. The colors of the points on the vertical line correspond to the respective colors of the Q_n curves.

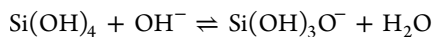
In the case of low silica concentration, we observed that the mass and mole average cluster sizes are quite similar, indicating a relatively monodisperse cluster distribution. These cluster sizes were found to decrease very gradually with an increase in the $\text{SDA}^+(\text{OH}^-)$ mole fraction. We also studied the PDDF of clusters under these conditions. The peak and the spread of the PDDF for silica were found to shift to lower distances as the $\text{SDA}^+(\text{OH}^-)$ concentration increased, consistent with the computed average cluster sizes. The difference between the PDDF of silica and the PDDF of silica + SDA^+ suggests that SDA^+ cations do not just surround the cluster, but are also contained to some extent within the cluster. To further investigate the formation mechanism of the nanoparticles, we studied the evolution of the Q_i distribution. Our results suggest a common form for the Q_i distribution that may be expected under many different conditions of silica polymerization.

We have also studied networks in a high silica concentration system with density comparable to that in sol–gel processing. We observed a gel regime at low and intermediate $\text{SDA}^+(\text{OH}^-)$ mole fractions. This regime is marked by the presence of percolating networks in our simulations. The MC sampling is slow in this region, indicating that the dense network imposes long relaxation times. The mass average and mole average cluster sizes differ significantly, indicating polydispersity of clusters under these conditions. As the $\text{SDA}^+(\text{OH}^-)$ mole proportion approaches that of the initial tetraethyl orthosilicate, we observe a nanoparticle regime that is marked by a sudden drop in the mass average cluster size. The resulting nanoparticles are smaller than those obtained under more dilute conditions of silica, a surprising result considering that a higher silica concentration might be expected to produce larger nanoparticles. The formation mechanism of these clusters, studied using the Q_i distribution, is similar to that in the low silica concentration system. The PDDF reflects percolating networks at low and intermediate $\text{SDA}^+(\text{OH}^-)$ mole fractions, whereas at sufficiently high $\text{SDA}^+(\text{OH}^-)$ concentrations, the PDDF shows a monodisperse nanoparticle phase.

This simple model provides significant insights into silica polymerization across a range of pH values and silica concentrations. In the future we plan to build on this work by investigating the formation of zeolites and zeolite analogues³⁰ through more detailed models of structure-directing agents.

APPENDIX: ESTIMATION OF PH

The prediction of pH with a change in composition is an important component in the study of such systems because of the complex chemistry involved. Here we solve the concentration of components and pH corresponding to the composition $y\text{TEOS}:x\text{SDA}(\text{OH}):z\text{H}_2\text{O}$. We assume that the OH^- , released from the dissociation of $\text{SDA}^+(\text{OH}^-)$, deprotonates silicic acid to form a singly ionized ionic silicate monomer according to the reaction



The initial mole fractions calculated for each component are given by

$$x_{\text{SN}}^0 = \frac{y}{2x + z + 5y} \quad x_{\text{SI}}^0 = 0$$

$$x_{\text{OH}^-}^0 = \frac{x}{2x + z + 5y} \quad x_{\text{H}_2\text{O}}^0 = \frac{z + 4y}{2x + z + 5y}$$

The numbers 2 and 5 in the denominators arise because we assumed that each TEOS molecule hydrolyzes into a molecule of silicic acid and four molecules of ethanol and that a molecule of $\text{SDA}^+(\text{OH}^-)$ dissociates into a molecule each of SDA^+ and OH^- . After the reaction attains equilibrium, we assume that the activities of the individual species are the same as their concentrations. At equilibrium the concentrations are related to the dissociation constant of the reaction by

$$K_D = \frac{x_{\text{SI}}x_{\text{H}_2\text{O}}}{x_{\text{SN}}x_{\text{OH}^-}}$$

In this calculation, we have assumed that the system is dilute but we do account for the change in water moles. We also take the value of $\text{p}K_a$ as 9.5 for the first deprotonation of silicic acid³⁴ and the value of $\text{p}K_w$ of water as 13.8. Furthermore, we have assumed that the concentration of water remains constant at a value of 55.6 mol/L.

We then assign a change, δ , in the moles of each species from their initial concentration. Thus, the equilibrium compositions become

$$x_{\text{SN}} = \frac{y - \delta}{2x + z + 4y} \quad x_{\text{SI}} = \frac{\delta}{2x + z + 5y}$$

$$x_{\text{OH}^-} = \frac{\delta}{2x + z + 5y} \quad x_{\text{H}_2\text{O}} = \frac{z + 4y + \delta}{2x + z + 5y}$$

Substituting these equations into the previous equation for K_D , we obtain a quadratic equation for δ . We then choose a value of δ that gives us a positive concentration for each species and next calculate the equilibrium composition of each species. The case of $x = 0$ can be treated by traditional acid–base equilibrium calculations, which results in $\text{pH} \approx 2.30$ at $x = 0$. The pH of the mixture, at nonzero x , is then computed by

$$\text{pH} = \text{p}K_w + \log\{[\text{H}_2\text{O}](x - \delta)\}$$

As mentioned earlier, we then consider the remaining OH^- part of the solvent. Hence, the pH of the system remains fixed at the initial value.

We now compare our pH calculations with the findings of Yang et al.¹⁰ They used a stirred hydrogen electrode to calculate the pH of the solution before the crystallization of silicalite-1 during the clear solution synthesis. Figure 15 shows the comparison of the pH values obtained from our calculations

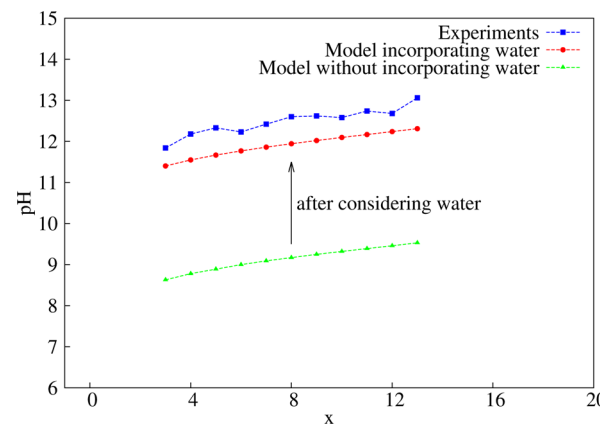


Figure 15. Computed pH values compared with those from experiments by Yang et al.¹⁰ at composition 25TEOS:xSDA(OH):480H₂O.

with those from the experiments. We observe good agreement with the experiments, indicating that we have captured much of the complex chemistry of the reactions successfully. However, it is evident that consideration of water moles in our calculations affects the results significantly.

AUTHOR INFORMATION

Corresponding Authors

*E-mail: auerbach@chem.umass.edu.

*E-mail: monson@ecs.umass.edu.

Notes

The authors declare no competing financial interest.

ACKNOWLEDGMENTS

This work was supported by a grant from the U.S. Department of Energy (Contract No. DE-FG02-07ER46466).

REFERENCES

- (1) Klein, L. C. *Sol-Gel Technology for Thin Films, Fibers, Preforms, Electronics, and Specialty Shapes*; Noyes Publications: Park Ridge, NJ, 1988.
- (2) Auerbach, S. M.; Carrado, K. A.; Dutta, P. K. *Handbook of Zeolite Science and Technology*; Marcel Dekker: New York, 2003.
- (3) Flanigen, E.; Bennett, J.; Grose, R.; Cohen, J.; Patton, R.; Kirchner, R.; Smith, J.; Silicalite, A. New Hydrophobic Crystalline Silica Molecular-Sieve. *Nature* **1978**, *271*, 512–516.
- (4) Davis, T.; Drews, T.; Ramanan, H.; He, C.; Dong, J.; Schnablegger, H.; Katsoulakis, M.; Kokkoli, E.; McCormick, A.; Penn, R.; Tsapatsis, M. Mechanistic Principles of Nanoparticle Evolution to Zeolite Crystals. *Nat. Mater.* **2006**, *5*, 400–408.
- (5) Schoeman, B. Analysis of the Nucleation and Growth of TPA-Silicalite-1 at Elevated Temperatures with the Emphasis on Colloidal Stability. *Microporous Mesoporous Mater.* **1998**, *22*, 9–22.
- (6) Watson, J.; Iton, L.; Keir, R.; Thomas, J.; Dowling, T.; White, J. TPA–Silicalite Crystallization from Homogeneous Solution: Kinetics and Mechanism of Nucleation and Growth. *J. Phys. Chem. B* **1997**, *101*, 10094–10104.
- (7) de Moor, P.; Beelen, T.; van Santen, R. In Situ Observation of Nucleation and Crystal Growth in Zeolite Synthesis. A Small-Angle X-ray Scattering Investigation on Si-TPA-MFI. *J. Phys. Chem. B* **1999**, *103*, 1639–1650.
- (8) Ravishankar, R.; Kirschhock, C.; Knops-Gerrits, P.; Feijen, E.; Grobet, P.; Vanoppen, P.; De Schryver, F.; Miehe, G.; Fuess, H.; Schoeman, B.; Jacobs, P.; Martens, J. Characterization of Nanosized Material Extracted from Clear Suspensions for MFI Zeolite Synthesis. *J. Phys. Chem. B* **1999**, *103*, 4960–4964.
- (9) Kragten, D.; Fedeyko, J.; Sawant, K.; Rimer, J.; Vlachos, D.; Lobo, R.; Tsapatsis, M. Structure of the Silica Phase Extracted from Silica/(TPA)OH Solutions Containing Nanoparticles. *J. Phys. Chem. B* **2003**, *107*, 10006–10016.
- (10) Yang, S.; Navrotsky, A.; Wesolowski, D.; Pople, J. Study on Synthesis of TPA-Silicalite-1 from Initially Clear Solutions of Various Base Concentrations by in Situ Calorimetry, Potentiometry, and SAXS. *Chem. Mater.* **2004**, *16*, 210–219.
- (11) Yang, S.; Navrotsky, A. Early-Stage Reactions in Synthesis of TPA–Silicalite-1: Studies by in Situ Calorimetry, SAXS, and pH Measurements. *Chem. Mater.* **2004**, *16*, 3682–3687.
- (12) Nikolakis, V.; Kokkoli, E.; Tirrell, M.; Tsapatsis, M.; Vlachos, D. Zeolite Growth by Addition of Subcolloidal Particles: Modeling and Experimental Validation. *Chem. Mater.* **2000**, *12*, 845–853.
- (13) Kumar, S.; Wang, Z.; Penn, R. L.; Tsapatsis, M. A Structural Resolution Cryo-TEM Study of the Early Stages of MFI Growth. *J. Am. Chem. Soc.* **2008**, *130*, 17284–17286.
- (14) Fedeyko, J.; Rimer, J.; Lobo, R.; Vlachos, D. Spontaneous Formation of Silica Nanoparticles in Basic Solutions of Small Tetraalkylammonium Cations. *J. Phys. Chem. B* **2004**, *108*, 12271–12275.
- (15) Parks, G. A. The Isoelectric Points of Solid Oxides, Solid Hydroxides, and Aqueous Hydroxo Complex Systems. *Chem. Rev.* **1965**, *65*, 177–198.
- (16) Carman, P. Constitution of Colloidal Silica. *Trans. Faraday Soc.* **1940**, *36*, 0964–0972.
- (17) Devreux, F.; Boilot, J.; Chaput, F.; Lecomte, A. Sol-Gel Condensation of Rapidly Hydrolyzed Silicon Alkoxides: A Joint Si-29 NMR and Small-Angle X-ray-Scattering Study. *Phys. Rev. A* **1990**, *41*, 6901–6909.
- (18) Malani, A.; Auerbach, S. M.; Monson, P. A. Probing the Mechanism of Silica Polymerization at Ambient Temperatures Using Monte Carlo Simulations. *J. Phys. Chem. Lett.* **2010**, *1*, 3219–3224.
- (19) Malani, A.; Auerbach, S. M.; Monson, P. A. Monte Carlo Simulations of Silica Polymerization and Network Formation. *J. Phys. Chem. C* **2011**, *115*, 15988–16000.
- (20) Jin, L.; Auerbach, S. M.; Monson, P. A. Modeling Three-Dimensional Network Formation with an Atomic Lattice Model: Application to Silicic Acid Polymerization. *J. Chem. Phys.* **2011**, *134*, 134703.
- (21) Brinker, C. J.; Scherer, G. W. *Sol-Gel Science: The Physics and Chemistry of Sol-Gel Processing*; Academic Press Inc.: Boston, MA, 1990.
- (22) Iler, R. *The Chemistry of Silica: Solubility, Polymerization, Colloid and Surface Properties, and Biochemistry*; John Wiley and Sons: New York, 1979.
- (23) Sefcik, J.; McCormick, A. Kinetic and Thermodynamic Issues in the Early Stages of Sol-Gel Processes Using Silicon Alkoxides. *Catal. Today* **1997**, *35*, 205–223.
- (24) Feuston, B.; Garofalini, S. Oligomerization in Silica Sols. *J. Phys. Chem.* **1990**, *94*, 5351–5356.
- (25) Garofalini, S.; Martin, G. Molecular Simulations of the Polymerization of Silicic Acid Molecules and Network Formation. *J. Phys. Chem.* **1994**, *98*, 1311–1316.
- (26) Rao, N.; Gelb, L. Molecular Dynamics Simulations of the Polymerization of Aqueous Silicic Acid and Analysis of the Effects of Concentration on Silica Polymorph Distributions, Growth Mechanisms, and Reaction Kinetics. *J. Phys. Chem. B* **2004**, *108*, 12418–12428.
- (27) Wu, M.; Deem, M. Monte Carlo Study of the Nucleation Process during Zeolite Synthesis. *J. Chem. Phys.* **2002**, *116*, 2125–2137.
- (28) Jorge, M.; Auerbach, S.; Monson, P. Modeling Spontaneous Formation of Precursor Nanoparticles in Clear-Solution Zeolite Synthesis. *J. Am. Chem. Soc.* **2005**, *127*, 14388–14400.
- (29) Jin, L.; Auerbach, S. M.; Monson, P. A. Simulating the Formation of Surfactant-Templated Mesoporous Silica Materials: A Model with Both Surfactant Self-Assembly and Silica Polymerization. *Langmuir* **2013**, *29*, 766–780.
- (30) Jin, L.; Auerbach, S. M.; Monson, P. A. Emergence of Zeolite Analogs and Other Microporous Crystals in an Atomic Lattice Model of Silica and Related Materials. *J. Phys. Chem. Lett.* **2012**, *3*, 761–765.
- (31) Follens, L. R. A.; Aerts, A.; Haouas, M.; Caremans, T. P.; Loppinet, B.; Goderis, B.; Verman, J.; Taulelle, F.; Martens, J. A.; Kirschhock, C. E. A. Characterization of Nanoparticles in Diluted Clear Solutions for Silicalite-1 Zeolite Synthesis Using Liquid ²⁹Si NMR, SAXS and DLS. *Phys. Chem. Chem. Phys.* **2008**, *10*, 5574–5583.
- (32) Auerbach, S.; Ford, M.; Monson, P. New Insights into Zeolite Formation from Molecular Modeling. *Curr. Opin. Colloid Interface Sci.* **2005**, *10*, 220–225.
- (33) Catlow, C.; Ackermann, L.; Bell, R.; Cora, F.; Gay, D.; Nygren, M.; Pereira, J.; Sastre, G.; Slater, B.; Sinclair, P. Computer Modelling as a Technique in Solid State Chemistry—Introductory Lecture. *Faraday Discuss.* **1997**, *106*, 1–40.
- (34) Sefcik, J.; McCormick, A. Thermochemistry of Aqueous Silicate Solution Precursors to Ceramics. *AIChE J.* **1997**, *43*, 2773–2784. Presented at the AIChE Topical Conference on Advanced Ceramics Processing as Part of the 5th World Congress of Chemical Engineering, San Diego, CA, July 1996.

- (35) Kinrade, S.; Swaddle, T. Si-29 NMR-Studies of Aqueous Silicate Solutions 0.2. Transverse Si-29 Relaxation and the Kinetics and Mechanism of Silicate Polymerization. *Inorg. Chem.* **1988**, *27*, 4259–4264.
- (36) Zana, R.; Yeager, E. Ultrasonic Vibration Potentials in Tetraalkylammonium Halide Solutions. *J. Phys. Chem.* **1967**, *71*, 4241–4244.
- (37) Caratzoulas, S.; Vlachos, D. G.; Tsapatsis, M. Potential of Mean Force for Tetramethylammonium Binding to Cagelike Oligosilicates in Aqueous Solution. *J. Am. Chem. Soc.* **2006**, *128*, 16138–16147.
- (38) Metropolis, N.; Rosenbluth, A.; Rosenbluth, M.; Teller, A.; Teller, E. Equation of State Calculations by Fast Computing Machines. *J. Chem. Phys.* **1953**, *21*, 1087–1092.
- (39) Hoshen, J.; Kopelman, R. Percolation and Cluster Distribution 0.1. Cluster Multiple Labeling Technique and Critical Concentration Algorithm. *Phys. Rev. B* **1976**, *14*, 3438–3445.
- (40) Rubinstein, M.; Colby, R. H. *Polymer Physics*; Oxford University Press: Oxford, U.K., 2003.
- (41) Harris, R.; Knight, C. Si-29 Nuclear Magnetic-Resonance Studies of Aqueous Silicate Solutions 0.5. 1st-Order Patterns in Potassium Silicate Solutions Enriched with Si-29. *J. Chem. Soc., Faraday Trans. 2* **1983**, *79*, 1525–1538.
- (42) Harris, R.; Knight, C. Si-29 Nuclear Magnetic-Resonance Studies of Aqueous Silicate Solutions 0.6. 2nd-Order Patterns in Potassium Silicate Solutions Enriched with Si-29. *J. Chem. Soc., Faraday Trans. 2* **1983**, *79*, 1539–1561.
- (43) Humphrey, W.; Dalke, A.; Schulten, K. VMD—Visual Molecular Dynamics. *J. Mol. Graphics* **1996**, *14*, 33–38.